Polycomb Repressive Complex 2 antagonizes linker DNA methylation and chromatin compaction in *Arabidopsis thaliana*

Martin Rougée*, Leandro Quadrana*, Jérôme Zervudacki*, Vincent Colot, Lionel Navarro and Angélique Deleris †

* These authors contributed equally to this work

† Correspondance : deleris@biologie.ens.fr

Institut de biologie de l'Ecole normale supérieure (IBENS), Ecole normale supérieure, CNRS, INSERM, PSL Research University, 75005 Paris, France

Abstract

In plants and mammals, DNA methylation is a hallmark of transposable element (TE) sequences that contributes to their epigenetic silencing. In contrast, histone H3 lysine 27 trimethylation (H3K27me3), which is deposited by the Polycomb Repressive Complex 2 (PRC2), is a hallmark of repressed genes. Nevertheless, there is a growing body of evidence for a functional interplay between these pathways. In particular, many TE sequences acquire H3K27me3 when they lose DNA methylation and it has been proposed that PRC2 can serve as a back-up silencing system for hypomethylated TEs. Here, we show in the flowering plant *Arabidopsis thaliana* that hundreds of TEs gain H3K27m3 in the mutant *ddm1*, which is defective in the maintenance of DNA methylation specifically over TE and other repeat sequences. Moreover, this gain depends solely on CURLY LEAF (CLF), which is one of two otherwise partially redundant H3K27 methyltransferases active in vegetative tissues. Finally, our results challenge the notion that PRC2 can be a compensatory silencing system for hypomethylated TEs, as the complete loss of H3K27me3 in *ddm1 clf* double mutant plants was not associated with further reactivation of TE expression nor with a burst of transposition. Instead, *ddm1 clf* plants exhibited a partial suppression of *ddm1* molecular phenotypes with with TE silencing, chromatin recompaction and hypermethylation of linker DNA compared to *ddm1*. Thus, we have uncovered a novel role for PcG in antagonizing both chromatin compaction and linker DNA methylation at pericentromeric TEs, which could be particularly important during the reproductive stage, when TE become hypomethylated in the pollen and the endosperm.

Introduction

DNA methylation is an epigenetic mark involved in the stable silencing of transposable elements (TEs) as well as the regulation of gene expression in plants and mammals. When present over TE sequences, it is usually associated with the di- or trimethylation of histone H3 lysine 9 (H3K9me2/H3K9me3) and, in plants, positive feedback loops between the two marks exist, which maintain TE sequences in the heterochromatic state (Johnson *et al*, 2002; Du *et al*, 2015). In *A. thaliana*, DOMAINS REARRANGED METHYLASE 2 (DRM2) establishes DNA methylation in all three sequences contexts (i.e. CG, CHG and CHH) in a pathway referred to as RNA-directed DNA methylation (RdDM) that involves small RNAs (Cao & Jacobsen, 2002; Chan, 2004). Maintenance of DNA methylation over TEs is achieved by the combined and context-specific action of RdDM (CHH methylation), CHROMOMETHYLASES 2 and 3 (CMT2 and CMT3, for CHH and CHG methylation, respectively) (Zemach *et al*, 2013; Stroud *et al*, 2014) and METHYLTRANSFERASE1 (MET1) (CG methylation) (Kankel *et al*, 2003). In addition, the SNF2 family chromatin remodeler DECREASE IN DNA METHYLATION 1 (DDM1) is necessary for DNA methylation of most TE sequences in all cytosine sequence contexts.

In contrast to DNA methylation, histone H3 lysine 27 trimethylation (H3K27me3), which is targeted by the highly conserved Polycomb Group (PcG) proteins, in particular Polycomb Repressive Complex 2 (PRC2), is a hallmark of transcriptional repression of protein-coding and microRNA genes in plants as well as in animals (Marasca *et al*, 2018; Förderer *et al*, 2016; Chica *et al*, 2017; Prete *et al*, 2015) ; it is thought to act by promoting a local compaction of the chromatin that antagonizes the transcription machinery (Prete *et al*, 2015) in order to maintain transcriptional silencing (Holoch & Margueron, 2017). Thus, H3K27me3 and DNA methylation are generally considered as mutually exclusive chromatin marks.

Nonetheless, there is a growing body of evidence of an interplay between the two silencing pathways. In particular, in both plants and mammals, many TE sequences gain H3K27me3 upon their loss of DNA methylation (Mathieu *et al*, 2005; Deleris *et al*, 2012; Saksouk *et al*, 2014; Reddington *et al*, 2013). Moreover, in the filamentous Neurospora, H3K27me3 is redistributed from gene to TE-rich constitutive heterochromatin when the heterochromatic mark H3K9me3 or the protein complexes that bind to it are lost (Basenko *et al*, 2015).

The fact that H3K27me3 can mark TE sequences upon their demethylation led to the idea that PcG could serve as a back-up silencing system for hypomethylated TEs (Deleris *et al*, 2012).

69 Consistent with this notion, subsequent work in mammals showed that H3K27me3 re-
70 established the repression of thousands of hypomethylated TEs in embryonic stem cells
71 subjected to rapid and extensive DNA demethylation (Walter *et al*, 2016).
72 In a previous study, we provided evidence supporting a role of PcG in the transcriptional
73 silencing of *EVD* (Zervudacki *et al*, 2018), an *A. thaliana* retroelement of the *ATCOPIA93*
74 family that is tightly controlled by DNA methylation and which transposes in plants mutated
75 for the chromatin remodeler *DDM1* (Tsukahara *et al*, 2009). We observed that silencing of *EVD*
76 is dependent on both DNA methylation and H3K27me3, which, at this locus, depends on the
77 SET-domain protein CURLY LEAF (CLF) (Zervudacki et al., 2018). Whether the dual control
78 observed at *EVD* is also present at other plant TEs is unknown.
79 In the present work, we integrated genetics, epigenomics and cell imaging to show that
80 numerous TEs gain H3K27me3 in response to *ddm1*-induced loss of DNA methylation. We
81 demonstrate also that this gain is mediated by CLF, with no role for the SET-domain H3K27
82 methyltransferase SWINGER (SWN), which is also active in vegetative tissues and otherwise
83 partially redundant with CLF (Chanvivattana *et al*, 2004; Wang *et al*, 2016; Yang *et al*, 2017).
84 Unexpectedly, the combination of *ddm1* and *clf* mutations was not associated with further
85 reactivation of TE expression or transposition as compared to *ddm1,* except for *EVD*. Instead
86 there was partial recompaction of heterochromatin in the double mutant. Accordingly, we also
87 observed DNA hypermethylation in *ddm1 clf* versus *ddm1,* prominently in linker DNA,
88 indicating that in the absence of *DDM1* activity, H3K27me3 antagonizes DNA methylation and
89 heterochromatin formation.
90
91 **Hundreds of hypomethylated TEs gain H3K27me3 in *ddm1***
92 We previously showed that in *met1* mutants impaired for CG methylation, hundreds of TEs
93 gain H3K27me3 methylation in Arabidopsis (Deleris *et al*, 2012). While *met1* and *ddm1*
94 mutants are both globally hypomethylated, the later, in contrast to the former, affects almost
95 exclusively TE and other repeat sequences, and in the three sequence contexts. Thus, the *ddm1*
96 mutant appeared to be a more relevant background to directly explore the interplay between
97 DNA methylation and Polycomb at TE sequences and we conducted a H3K27me3 ChIP-seq
98 experiment in this mutant. Like in *met1*, hundreds of TEs showed increased accumulation of
99 H3K27me3 in *ddm1* (**Figure 1A-C**). A stringent subset of 672 TEs showed no H3K27me3
100 ChIP-seq signal in wild-type plants and significantly gained H3K27me3 over their full length
101 in *ddm1* (**Figure 1D**). Moreover, the vast majority of those 672 TEs are located in
102 pericentromeric regions (**Figure 1E**) and were included in the subset of TEs that gain

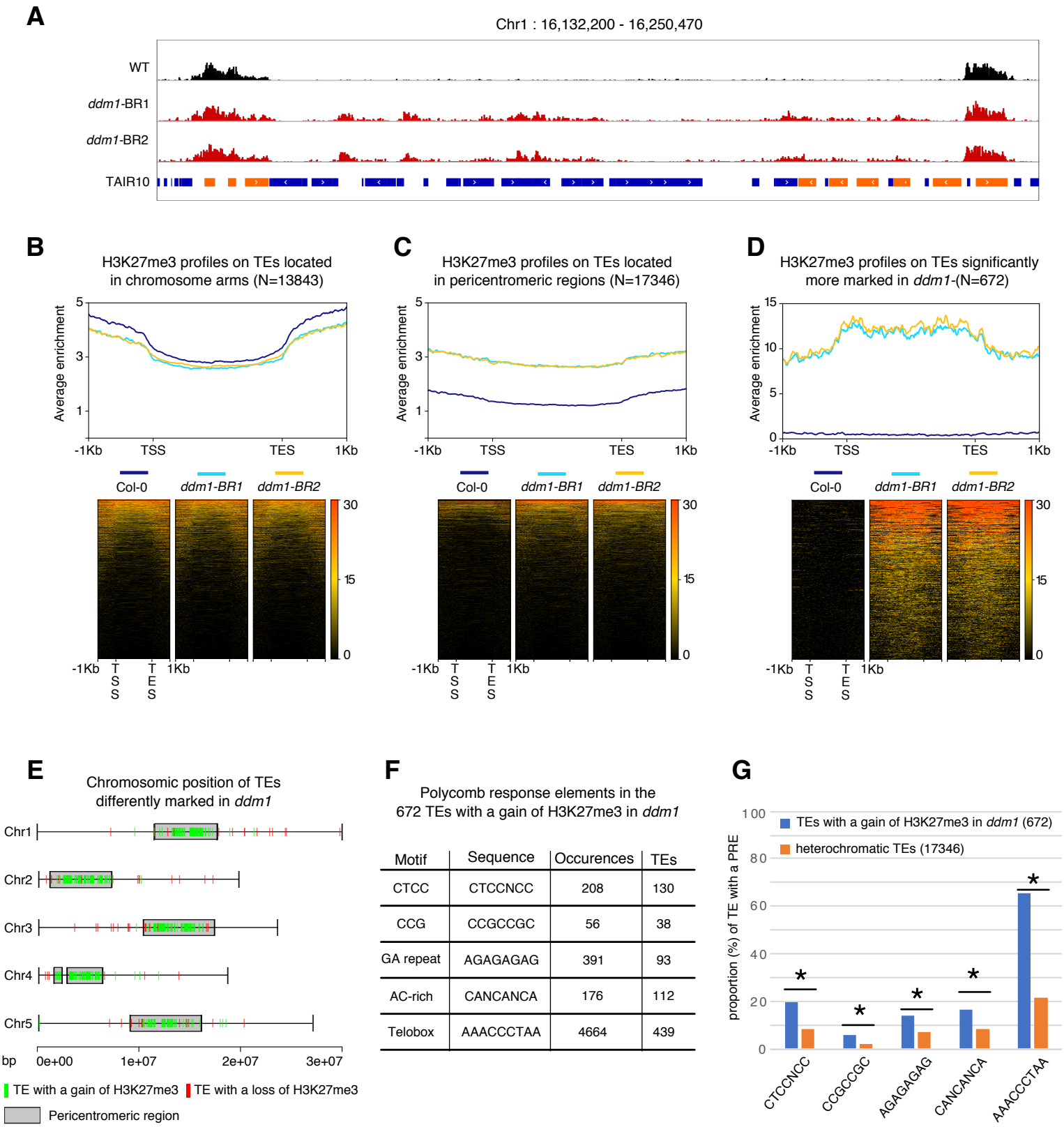

Motif	Sequence	Occurences	TEs
CTCC	CTCCNCC	208	130
CCG	CCGCCGC	56	38
GA repeat	AGAGAGAG	391	93
AC-rich	CANCANCA	176	112
Telobox	AAACCCTAA	4664	439

Figure 1. A mutation in *DDM1* leads to a gain of H3K27me3 on some heterochromatic TEs.
(**A**) Representative genome browser view of H3K27me3 levels in a 100 kb heterochromatic region of chromosome 1 in wild-type (WT) and two biological replicates (BR) of *ddm1* (blue bar: TE; orange bar: gene). (**B,C,D**) H3K27me3 enrichment in WT, *ddm1*-BR1 and *ddm1*-BR2 over TEs located in euchromatin (**B**), heterochromatin (**C**) and TEs with a significant positive fold change (FC) of H3K27me3 in *ddm1* (Pval<0,1 ; Log 2FC>2) (**D**). The upper graph shows the mean enrichment of H3K27me3 over a given TE subset; the corresponding heatmap below ranks them from top to bottom according to the average enrichment in all genotypes. (**E**) Chromosomal distribution of the 672 TEs that significantly gain H3K27me3 (Pval<0,1 ; Log2FC>2) and the 61 TEs that significantly lose H3K27me3 in *ddm1* (Pval<0,1 ; Log2FC<-2). (**F**) Table showing the occurences of Polycomb Response Elements (PRE) (Xiao et al., 2017) among the 672 TEs with a gain of H3K27me3 in *ddm1*. (**G**) Graph showing the proportion of TEs (TEs with a gain of H3K27me3 in *ddm1* compared to heterochromatic TEs) with a given PRE.

103 H3K27me3 in *met1* (Deleris *et al*, 2012) (**Figure supplement 1A**). Four major TE super
104 families were overrepresented among the 672 TEs (LTR/Gypsy, LTR/Copia, DNA/En-Spm,
105 DNA/others) (**Figure supplement 1B**), suggesting the existence of sequence-specific targeting.
106 Indeed, PRC2 can be targeted to specific genes by the recognition of short sequence motifs
107 (Xiao et al., 2017). Consistent with this motif-based targeting, we detected a significant
108 enrichment of the Telobox, CTCC, GA-repeat and AC-rich motifs in the 672 TEs compared to
109 the rest of the heterochromatic TEs (**Figure 1F-G**). These results suggest the presence of an
110 instructive mechanism of PRC2 recruitment at TEs with particular motifs used as nucleation
111 sites. In addition, the detection of continuous blocks of H3K27me3, in particular on
112 chromosomes 1 and 4 (**Figure supplement 1C**), may suggest that, once nucleated, H3K27me3
113 domains spread over entire TE sequences and even beyond, into nearby TEs, in a fashion similar
114 to what was described at genic sequences (Yang *et al*, 2017; Wang *et al*, 2016).
115
116 **The gain of H3K7me3 over hypomethylated TEs depends on CLF**
117 To test whether CLF is required for the gain of H3K7me3 over TEs we performed a second set
118 of ChIP-seq experiments in *ddm1 clf.* Because total levels of H3K27me3 are strongly reduced
119 in both *clf* and *ddm1 clf* mutants (**Figure supplement 2A**) compared to wild-type, we spiked-
120 in exogenous Drosophila chromatin in the chromatin extracts for normalization (Orlando *et al*,
121 2014). Levels of H3K27me3 at genes were similar between *ddm1 clf* and *clf* mutant (**Figure**
122 **supplement 2B**), consistent with *DDM1* affecting TE and other repeat sequences specifically
123 (Lippman *et al*, 2004). Conversely, the gain of H3K27me3 observed over TEs in *ddm1* was
124 completely abolished in *ddm1 clf* (**Figure 2A-C**). Together, these results show that deposition
125 of H3K27me3 at most TEs in *ddm1* is fully dependent on *CLF*. This is in contrast with the well-
126 established, partial dependency of H3K27me3 deposition at genes on CLF (Wang *et al*, 2016;
127 Yang *et al*, 2017), which has been proposed to be due to a specialization of this factor in
128 mediating amplification and spreading of H3K27me3 marks after their establishment by SWN
129 (Yang *et al*, 2017). Thus, at least over *ddm1*-dependent hypomethylated TEs, CLF is required
130 for the nucleation, and perhaps, additionally, spreading of H3K27me3.
131
132 **TE activation in *ddm1* is partially suppressed in *ddm1 clf***
133 We previously described the phenotype of *ddm1 clf* plants at the rosette stage (4.5 weeks-old).
134 By observing the plants at the seedling stage (15 days-old), we could observe additional
135 phenotypes in two out of three independent *ddm1 clf* lines (chlorosis in one line, growth arrest
136 in another) that segregated 1:3 and thus evoked the segregation of recessive mutations (**Figure**

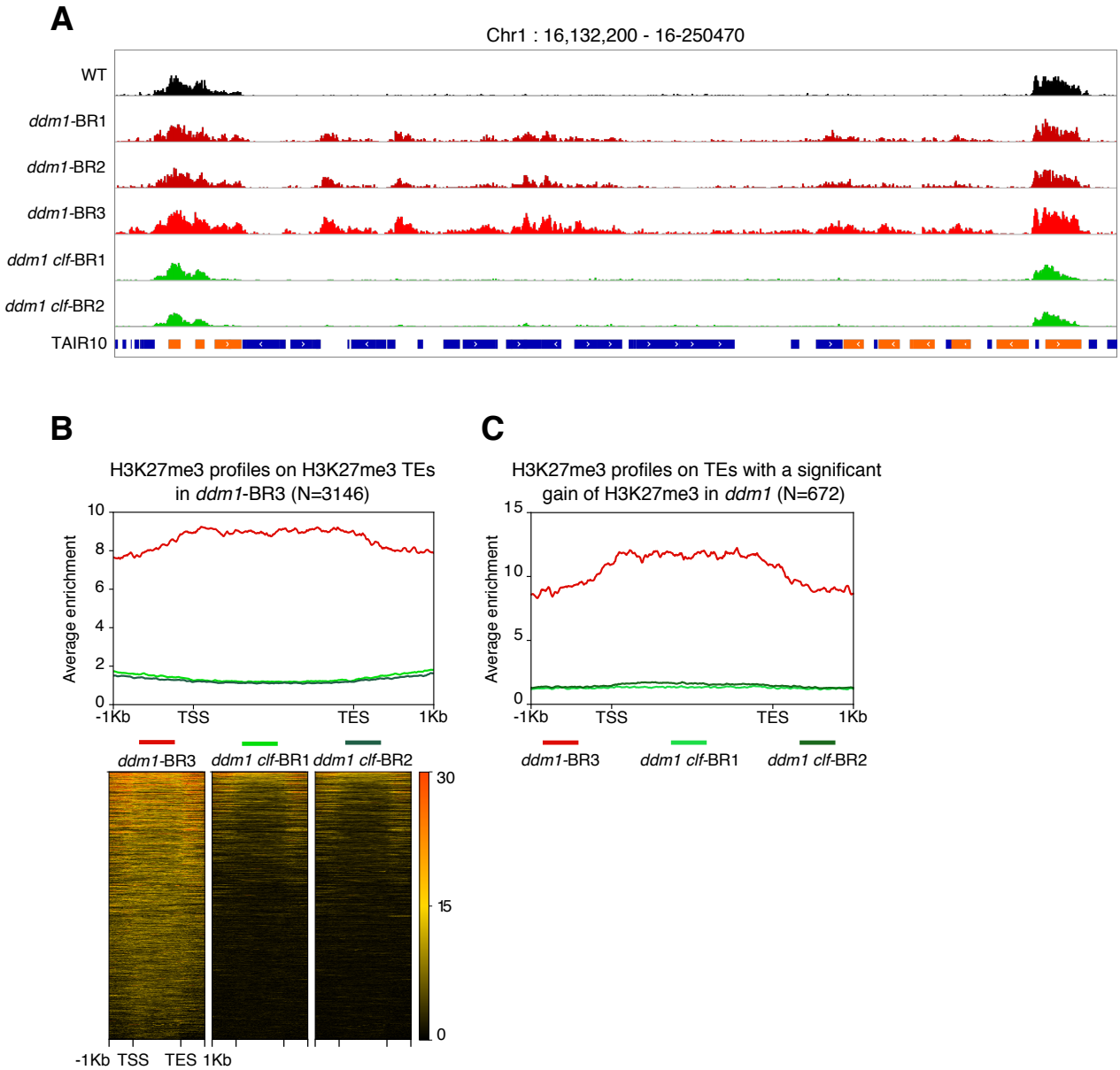

Figure 2. The gain of H3K27me3 in *ddm1* is completely lost in *ddm1 clf*.
(**A**) Genome browser view of H3K27me3 levels on the same region as Figure 1 (**B**) H3K27me3 enrichment in *ddm1* and two *ddm1 clf* replicates over TEs with a H3K27me3 domain in *ddm1* with corresponding heatmap ranking TEs according to the H3K27me3 mean value. (**C**) Metagene representing H3K27me3 enrichment in *ddm1*-BR3, *ddm1 clf*-BR1 and *ddm1 clf*-BR2 of the 672 TEs previously shown to gain H3K27me3 in *ddm1.*

137 **3A**). We previously showed that there is an enhanced accumulation of *ATCOPIA93* mRNAs in
138 *ddm1 clf* double mutant as compared to *ddm1* (Zervudacki et al., 2018), thus we hypothesized
139 that these segregating phenotypes were caused by the transposition of TEs activated in *ddm1*
140 *clf.*
141 To test whether *ATCOPIA93* activity is increased and whether additional copies of this TE
142 family accumulate in *ddm1 clf*, we performed Southern blot analysis (**Figure 3B**) using a probe
143 specific of *ATCOPIA93 EVD*/*ATR* (*ATR* is an almost identical copy of *EVD*). In the wild-type
144 as well as the *ddm1* and *clf* single mutants, we could only observe one copy of *EVD* and *ATR*.
145 By contrast, we observed linear extrachromosomal DNA in all the *ddm1 clf* double mutant lines
146 tested (progenies of individual F2), consistent with previous results (Zervudacki *et al*, 2018).
147 In addition, in two out of three double mutant lines, we detected numerous additional bands
148 corresponding to *EVD*/*ATR* new insertions (**Figure 3B**), indicating that transposition occurs in
149 the double mutant, although to various extents which may reflect different dynamics of
150 mobilization following the initial event (Quadrana *et al*, 2019). Pyrosequencing performed on
151 the mutants showed that *ATCOPIA93* DNA (extrachromosomal and integrated) was mostly
152 contributed by *EVD* (**Figure 3C**). Thus, DNA methylation and H3K27me3 act in synergy to
153 negatively control *EVD* activity and prevent its transposition, in accordance with the dual
154 control they exert on its transcription (Zervudacki *et al*, 2018). To test whether more TEs are
155 activated in *ddm1 clf*, we performed TE-sequence capture (Quadrana *et al*, 2016), which
156 enables sensitive detection of new TE insertions at the genome wide-level, in about 100
157 seedlings of wild-type, *ddm1* (2nd generation inbred mutants) and *ddm1 clf* (F3 progenies). No
158 new insertions were detected for any of the 250 TEs tested in this manner, except for *EVD*,
159 which had accumulated more copies in *ddm1 clf* than in *ddm1* (**Figure 3D)***,* although this
160 difference was not statistically significant in average — this was presumably because the *ddm1*
161 *clf* line (#1), where only ecDNA accumulates, was included in the experiment along lines #2
162 and #3 **(Figure supplement 3A**).
163 To investigate further the relationship between H3K27me3 and TE silencing, we performed
164 RNA-seq experiments in three and four biological replicates of *ddm1* and *ddm1 clf*,
165 respectively. In all *ddm1*, about a thousand TEs (929) were upregulated, the large majority of
166 which (865) did not show a significant gain of H3K27me3 marks in this background. We found
167 that a similar (*ddm1 clf*-BR3/4) or even lower (*ddm1 clf*-BR1/2) number of TEs were
168 transcriptionally active in *ddm1 clf* compared to *ddm1* (**Figure 3E**) in keeping with the lack of
169 enhanced transposition in *ddm1 clf.* Moreover, among the 1957 TEs that lose H3K27me3 in
170 *ddm1 clf*, we found only 14 TEs that were upregulated in all *ddm1 clf* lines versus *ddm1* (**Figure**

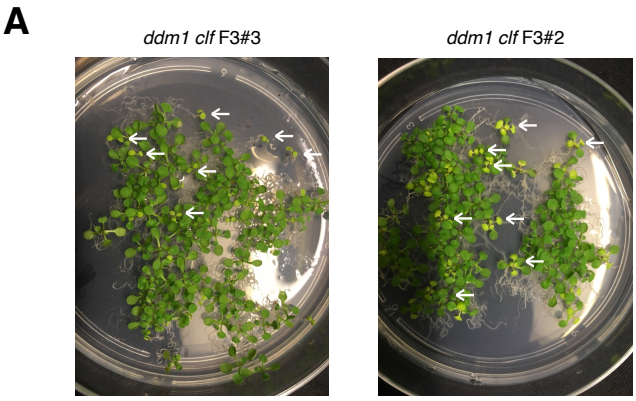

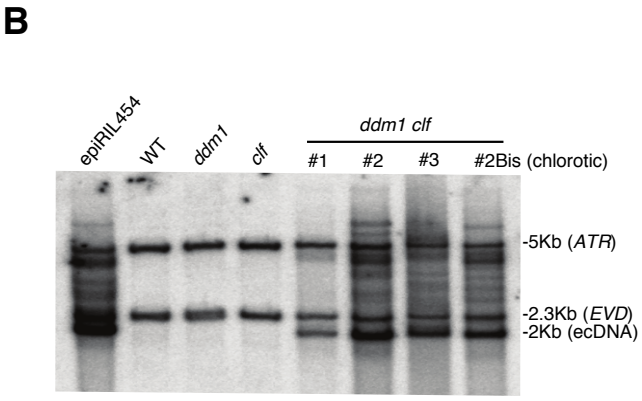

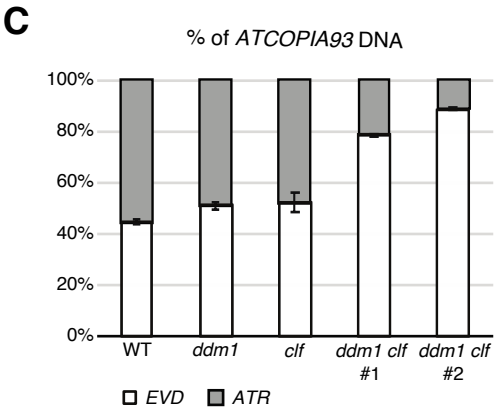

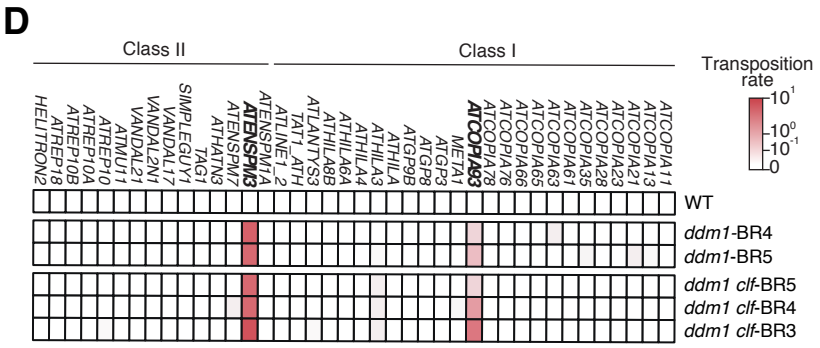

E

Genotype	Up-regulated TE	Down-regulated TE
ddm1	1024	1
ddm1- BR4	1113	1
ddm1- BR3	1085	4
ddm1 clf- BR1	327	0
ddm1 clf- BR2	601	0
ddm1 clf- BR3	1000	1
ddm1 clf- BR4	970	0

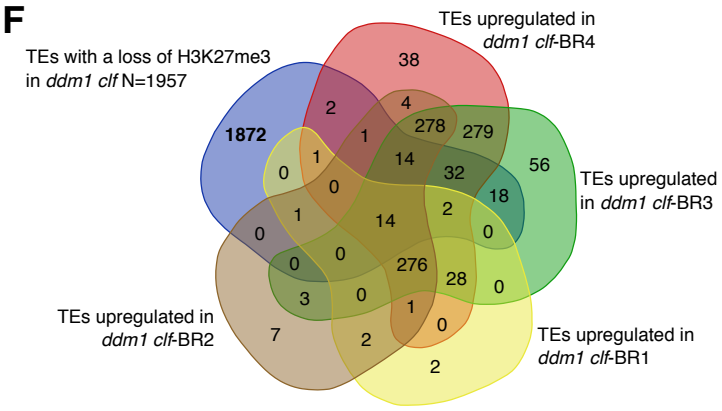

Figure 3. Transposons activation in *ddm1* and *ddm1 clf*.
(**A**) Representative picture of 15 days-old *ddm1 clf* F3 seedlings coming from two independent F2 lines; the white arrows show two different phenotypes segregating 1:3, growth arrest (left) and chlorosis (right) respectively. (**B**) Southern blot analysis on a pool of leaves (8 rosettes for each genotype), using an *ATCOPIA93* probe that recognizes both *EVD* and *ATR* copies; epiRIL454 (Mari-Ordonez et al., 2013) was used as a positive control for activation of *ATCOPIA93* and three independent *ddm1 clf* lines were tested. (**C**) Qualitative analysis of genomic DNA by pyrosequencing. The position interrogated corresponds to the discriminating SNP between *EVD* (C/G) and *ATR* (A/T) and the % indicated represent the % of G (*EVD*, white bar) or T (*ATR*, grey bar) (**D**) Heatmap showing the transposition rates of 40 potentially mobile TEs as determined by TE-capture (Quadrana et al., 2016) using 100 seedlings for each genotype. (**E**) Table showing up-regulated and down-regulated TEs compared to WT as identified by RNA-seq analyses on seedlings. (**F**) Venn diagram showing the overlap between TEs with a loss of H3K27me3 in *ddm1 clf* and TEs up-regulated in the 4 different *ddm1 clf* lines.

171 **3F**). Thus, with the exception of *EVD* case study, which supports our initial hypothesis of a
172 dual epigenetic control by DNA methylation and H3K27me3, it appears that *ddm1*-induced
173 activation of TEs is partially suppressed in *ddm1 clf,* with some heterogeneity between the lines
174 used.
175
176 **H3K27me3 antagonizes *ddm1*-induced chromatin decompaction and DNA methylation**
177 **loss**
178 To understand the mechanisms underlying the antagonism between DNA methylation and
179 *CLF*-dependent H3K27me3 deposition, we performed cytogenetic analyses on nuclei from
180 single and double mutants for *DDM1* and *CLF.* Chromocenters formation and DNA compaction
181 were unchanged in *clf* but strongly impacted in *ddm1* as previously published (Soppe *et al*,
182 2002). By contrast, they were only partially affected in the double mutant, indicating that
183 H3K27me3 loss induces chromatin recompaction specifically in the *ddm1* background (**Figure**
184 **4A**). In addition, immunofluorescence experiments showed that this chromatin recompaction
185 was associated with the recovery of H3K9me2 distribution (**Figure 4B**).
186 In order to assess whether chromatin recompaction associates with DNA methylation gain, we
187 compared the DNA methylomes of *ddm1* and *ddm1 clf* mutant plants. Consistent with the
188 cytogenetic analyses, hundreds of loci exhibited higher DNA methylation in all three sequence
189 contexts in *ddm1 clf* compared to *ddm1* (**Figure 5A**), with gains being most pronounced at
190 CHH sites and variable from one line to the other (**Figure 5B**). Furthermore, TEs with increased
191 CG methylation in *ddm1 clf* versus *ddm1* were slightly but statistically significantly less
192 expressed compared to those that did not show such an increase in this mutant background
193 (**Figure supplement 5A**).
194 To test whether H3K27me3 antagonizes *ddm1*-induced DNA methylation loss in *cis*, we
195 searched for differential methylated regions (DMRs) using non-overlapping 100bp windows.
196 There were few hyper DMRs and these tended to be inconsistent across replicates, suggesting
197 that they were the result of stochastic variation of DNA methylation (Becker *et al*, 2011).
198 Moreover, TEs showing clear DNA methylation gain in *ddm1 clf* compared to *ddm1* (**Figure**
199 **5A**) were not identified by our DMR detection. Visual inspection of these DNA
200 hypermethylated TEs revealed that increased DNA methylation was in fact confined to short
201 sequences (~20bp), typically separated by ~140 bp (**Figure supplement 5B**). Indeed, we
202 identified 1208 TE-specific short (20bp) sequences with higher CG methylation in *ddm1 clf*
203 compared to *ddm1*. These small-size hyper-DMRs were distributed over 759 TEs, most of
204 which (N= 571) are pericentromeric, and they were associated with a reduction of H3K27me3

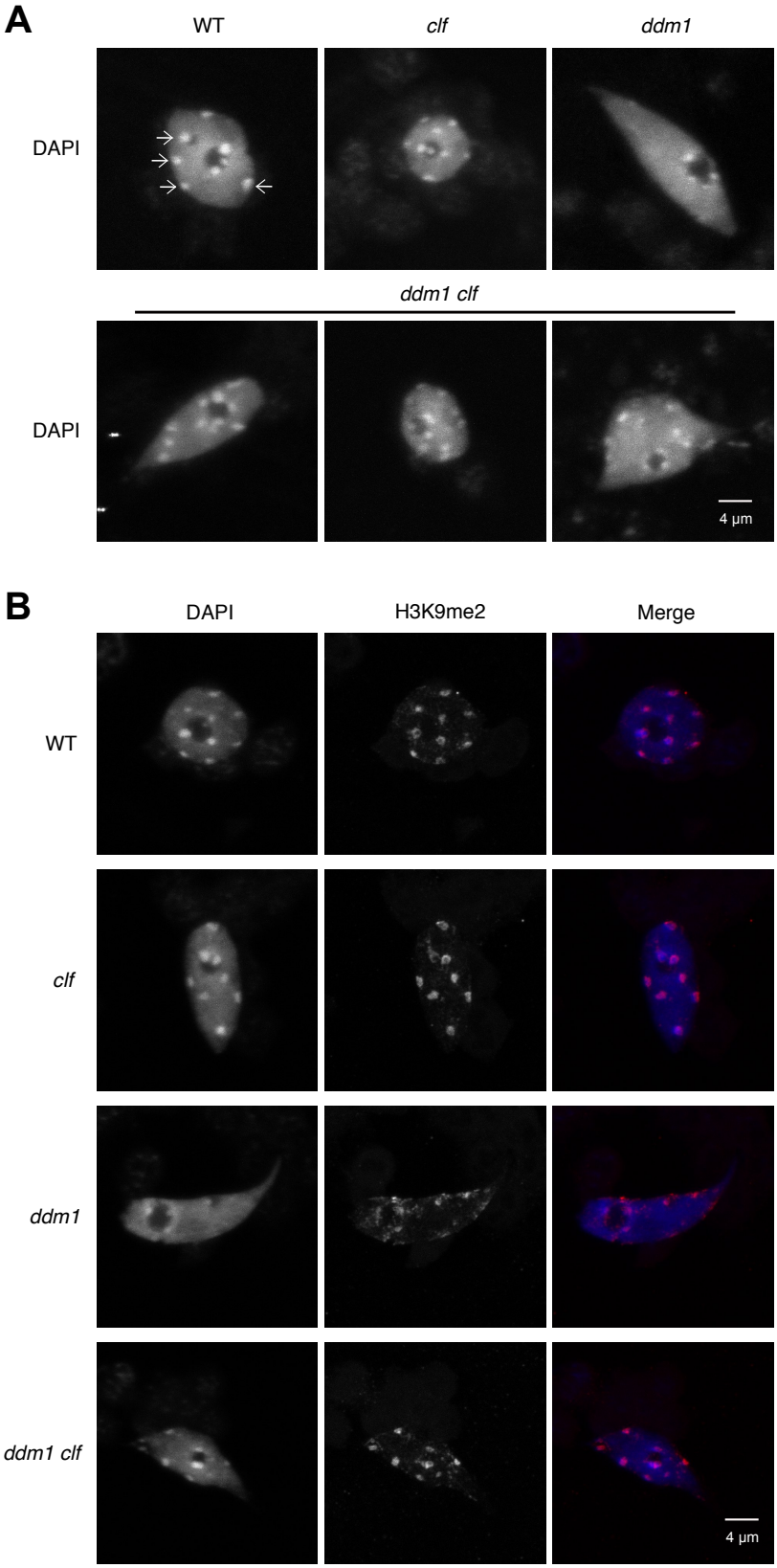

Figure 4. The double mutant *ddm1 clf* displays a partial recompaction of DNA and more visible H3K9me2 compared to *ddm1*.

(**A**) Representative picture of DAPI stained nuclei extracted from 50 fixed 10 days-old Arabidopsis seedlings for each genotype (three independent F3 lines from *ddm1 clf*) (**B**) Representative picture of DAPI staining and H3K9me2 immunodetection of nuclei extracted from 50 fixed 10 days-old Arabidopsis seedlings for each genotype.

levels (**Figure 5C,** H3K27me3 profiles centered on CG-DMRs), consistent with an antagonism between H3K27me3 and DNA methylation. Among these 759 TEs hypermethylated in *ddm1 clf* compared to *ddm1*, 61 showed a significant gain of H3K27me3 in *ddm1:* this is a significant 3.8 representation factor enrichment ($p<3.644e^{-19}$) compared to the number of TEs in the genome that would be both CG-hypermethylated (in *ddm1 clf*) and H3K27me3-marked (in *ddm1*) by chance. This observation suggests that there is a direct antagonism between H3K27me3 marks in *ddm1* and DNA methylation gains in *ddm1 clf,* at least at a subset of pericentromeric TEs. However, we do not exclude an additional and/or alternative indirect antagonism mediated for instance by H3K27me3-dependent chromatin decompaction.

Finally, the ~140 bp distance between DMRs at discrete loci —which is roughly the size of nucleosomal DNA— prompted us to test whether DNA hypermethylation in *ddm1 clf* versus *ddm1* occurred preferentially between nucleosomes. Analysis of publicly available MNase data obtained for *ddm1* (Lyons & Zilberman, 2017) indicated that the periodic DNA hypermethylation in *ddm1 clf* associate with linker DNA (**Figure 5C)**, consistent with *in vitro* and *in vivo* data showing that inter-nucleosomal DNA is more accessible to DNA methyltransferases than DNA bound to the nucleosome core particle (Lyons & Zilberman, 2017). These findings suggest therefore that CLF-dependent H3K27me3 marks limit the accessibility of DNA methyltransferases to linker DNA.

Discussion

In this study, we have shown that hundreds of TEs gain H3K27me3 when hypomethylated by *ddm1*. This phenomenon has two important mechanistic implications, the first one being that DNA methylation can globally exclude H3K27me3. We and others previously showed that loss of DNA methylation induced by another hypomethylation mutant, *met1*, rather than loss of H3K9me2, allows for H3K27me3 deposition at TEs (Mathieu *et al*, 2005; Deleris *et al*, 2012). However, another commonality between *met1* and *ddm1* mutants is the decompaction of their DNA, which could also contribute to favor the access of PRC2 to chromatin, a possibility that could be further investigated by identifying and using genetic backgrounds impaired for chromatin compaction but not DNA methylation. The second mechanistic implication of our observations is that PRC2 can be recruited to TEs. Here, we have characterized the transposons marked by H3K27me3 in *ddm1* and found some motifs recently described in the genic targets of PRC2 and functionally involved in the recruitment of this complex at genes (Xiao *et al*, 2017). Thus, while some TEs could be marked by H3K27me3 due to spreading from adjacent

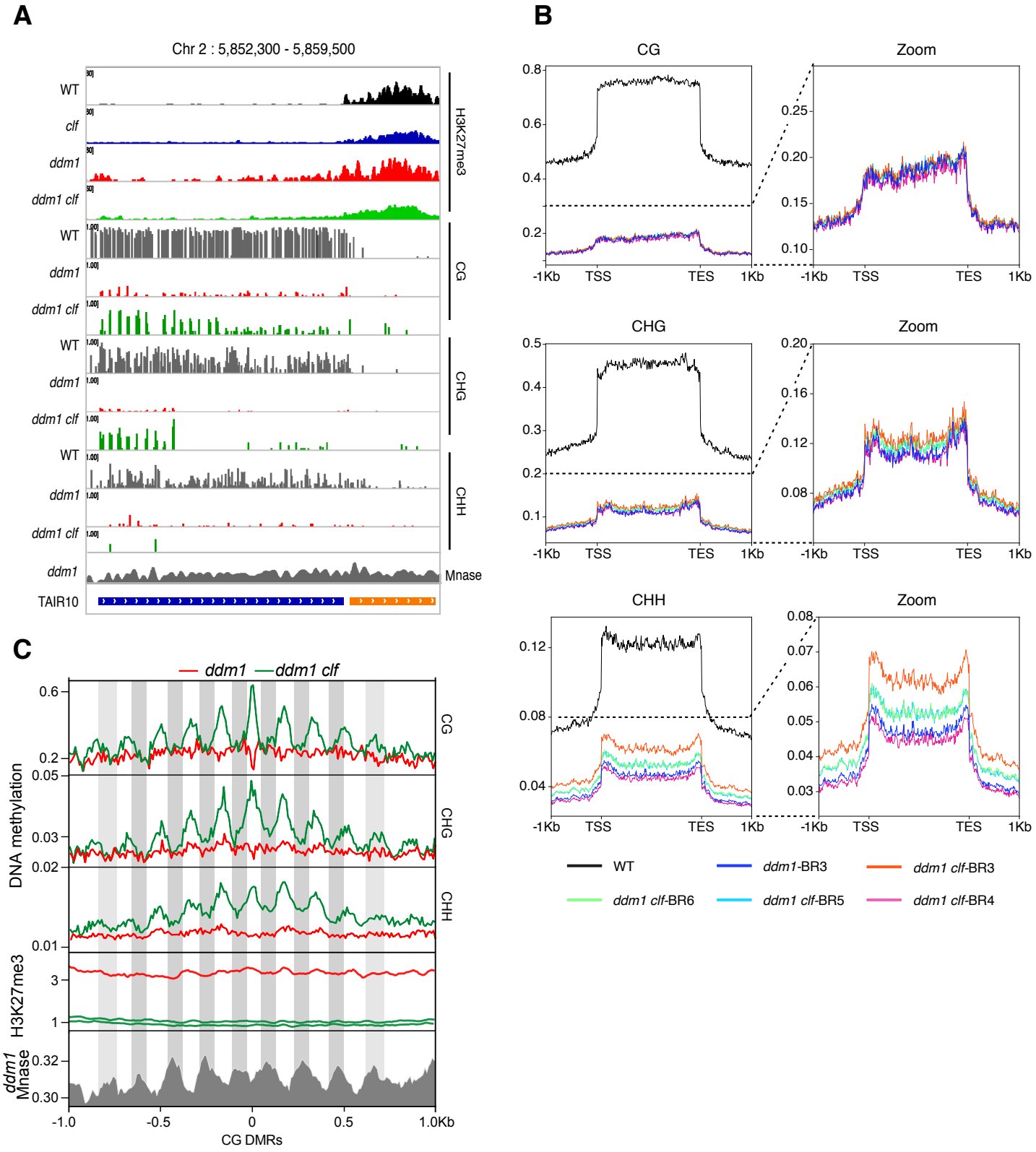

Figure 5. Periodic hypermethylation is observed in *ddm1 clf* compared to *ddm1*.
(**A**) Representative genome browser view of H3K27me3 and methylation of a TE (blue bar) showing hypermethylation in *ddm1 clf* compared to *ddm1*. (**B**) Meta-TEs showing average DNA methylation levels on all TEs, in the three different contexts, in all the genotypes of interest, with a zoom on *ddm1* and *ddm1 clf* methylated TEs. (**C**) Plot showing average DNA methylation, H3K27me3 and nucleosome occupancy (every peak in *ddm1* Mnase data shows the position of a nucleosome) 1Kb upstream ans downstream of "small" CG DMRs (20bp) in the three different sequence contexts.

239 PcG targets as it is the case for *EVD* (Zervudacki et al., 2018), the presence of these motifs as
240 well as the localization of many TEs far away from any H3K27me3 domain, suggests a
241 sequence-based, instructive mode of *cis*-recruitment for PRC2. Alternatively, this recruitment
242 could also be promoted by the enrichment of H2A.Z over demethylated TEs (Zilberman *et al*,
243 2008) since a mechanistic link was found between H2A.Z and H3K27me3 (Carter *et al*, 2018).
244 These non mutually exclusive scenarios will deserve future investigation.
245 Subsequently, the compound mutant of DNA methylation and PRC2, *ddm1 clf*, uncovered
246 unexpected and interesting molecular phenotypes. First, PRC2 targeting of TEs in the *ddm1*
247 background depends almost completely on CLF. This requirement of CLF contrasts with the
248 partial dependency on CLF and SWN at H3K27me3 marked genes, where SWN plays a major
249 role, presumably in nucleating H3K27me3 (Yang *et al*, 2017). A possible explanation for this
250 result could be that the transcription factors implicated in the nucleation of H3K27me3 (Xiao
251 *et al*, 2017) at TEs in *ddm1* recruit a FIE-EMF2-PRC2 complex that does not contain SWN.
252 Secondly, and from a functional point of view, our results challenge the idea that PRC2 acts as
253 a back-up silencing system in the absence of DNA methylation. Rather, they are reminiscent of
254 the observations made in Neurospora where the gain of H3K27me3 in constitutive
255 heterochromatin domains is not compensatory for gene silencing upon loss of H3K9
256 methylation (or its reader HP1) but rather leads to growth defects and altered sensitivity to
257 genotoxic agents (Basenko *et al*, 2015). In our study, in *ddm1 clf*, the loss of H3K27me3 did
258 not enhance the number of *ddm1*-activated TEs. Instead, molecular phenotypes of partial *ddm1*
259 suppression were observed: same or lesser number of activated TEs and partial compaction of
260 DNA compared to *ddm1* associated with hypermethylation of the DNA in the three sequence
261 contexts, which presumably results in transcriptional TE silencing. Thus, H3K27me3 appears
262 to antagonize DNA methylation and compaction in a *ddm1* background, which is reminiscent
263 of the described role of PcG in promoting hypomethylation of DNA methylation valleys in
264 mammals (Li *et al*, 2018). We propose two possible mechanisms for partial hypermethylation
265 of *ddm1 clf* compared to *ddm1* that could be explored in future work. Firstly, it is likely that in
266 *ddm1* mutant, like in *met1* (Zilberman *et al*, 2008), H2AZ is incorporated at TEs. H2AZ is
267 known to be antagonistic to DNA methylation and given that a mutation of *CLF* leads to loss
268 of H2AZ (Carter *et al*, 2018), this may favor the reestablishment of DNA methylation.
269 Secondly, we envision that DNA compaction in *ddm1 clf* promotes DNA methylation in a non-
270 specific manner thus providing an explanation for the widespread DNA hypermethylation of
271 TEs compared to *ddm1*. In a non-exclusive manner, small RNAs could also participate in either
272 of these processes. What favors DNA compaction upon loss of H3K27me3, and, accordingly

273 what antagonizes chromocenters formation in *ddm1* in the presence of H3K27me3 is also
274 unclear. It could be linked to the replacement of H3.1, the substrate for ATRX5 and 6 and
275 H3K27 monomethylation (a modification associated with chromatin condensation) (Jacob *et*
276 *al*, 2009, 2010) by H3.3 and H3K27me3 in *ddm1*, and the subsequent reincorporation of H3.1
277 in the absence of CLF. In this respect, the *ddm1 clf* mutant represents a valuable system to test
278 the causal and functional relationship between DNA methylation and DNA compaction, which
279 is elusive.
280 Finally, our work in *ddm1 clf* mutant could have important implications for biological situations
281 where TEs are naturally hypomethylated, DDM1 absent and/or chromatin decompacted. First,
282 in the pollen vegetative nucleus, where thousands of TEs are DNA-demethylated due to the
283 activity of DEMETER glycosylases (Ibarra *et al*, 2012), where DDM1 is not detected (Slotkin
284 *et al*, 2009). TE activation in this cell type is contributed by chromatin decondensation and
285 DNA demethylation-dependent and independent mechanisms (He *et al*, 2019) and has been
286 proposed to reinforce silencing in the gamete through production of small RNAs that could
287 transit into the sperm cell (Slotkin *et al*, 2009; Calarco *et al*, 2012; Ibarra *et al*, 2012; Martínez
288 *et al*, 2016). Whether PRC2 targets some of the demethylated TE-sequences and whether this
289 could antagonize chromatin decondensation and modulate TE activation and small RNA
290 production in this context is an open question. In this scenario, the mechanisms we have
291 described in this work could play an important role in the reinforcement of silencing in the
292 gametes and its modulation. Similarly, in the endosperm, the nutritive terminal tissue
293 surrounding the seed and derived from the central cell, the chromatin is less condensed than in
294 other types of nuclei (Baroux *et al*, 2007). In addition, thousands of TEs of the maternal genome
295 are naturally hypomethylated forming primary imprints and many of these hypomethylated TEs
296 are targeted by PRC2 forming secondary imprints (Weinhofer *et al*, 2010; Rodrigues &
297 Zilberman, 2015). These secondary imprints cause, for instance, the silencing of the maternal
298 *PHERES* locus while the cognate paternal allele is activated (Makarevich *et al*, 2008; Rodrigues
299 & Zilberman, 2015). The interplay between DNA methylation and PRC2 that we have
300 evidenced could thus be particularly relevant in this cell type and modulate the imprinting of
301 some genes. Finally, an exciting possibility is that PRC2 could target transposons after their
302 mobilization and integration and this could slow down the establishment of their DNA
303 methylation-based transgenerational and stable epigenetic silencing.
304
305
306

307 **Material and methods**
308

309 **Plant material and growth condition**

310 14 day-old seedlings grown on MS plates and with an 8h light/16h dark photoperiod were used
311 throughout the study except for Southern Blot where analyses were performed on 5-week-old
312 rosette leaves grown in the same conditions.
313

314 **Mutant lines**

315 We used the *ddm1-2* allele (Vongs *et al*, 1993) and the *clf-29* allele (Bouveret *et al*, 2006).
316 Double *ddm1 clf* mutants were generated by crossing the above-mentioned mutants (Zervudacki
317 *et al*, 2018). Experiments were performed on F3 progenies using *ddm1*-2 2nd generation plants
318 as controls.

319 **SDS-PAGE and Western blotting**

320 Chromatin-enriched protein fraction was extracted from 10-days-old seedlings as described in
321 (Bourbousse *et al*, 2012), quantified by standard BCA assay and 20 µg were resolved on
322 SDS/PAGE. After electroblotting the proteins on a Polyvinylidene difluoride (PVDF)
323 membrane, H3K27me3 analysis was performed using an antibody against the H3K27me3
324 (Millipore, 07-449) at a 1:1000 dilution and a secondary antibody against rabbit coupled to
325 HRP (Promega W4011) at a 1:20 000 dilution.

326 **BS-seq libraries**

327 DNA was extracted using a standard CTAB protocol. Bisulfite conversion, BS-seq libraries and
328 sequencing (paired-end 100 nt reads) were performed by BGI Tech Solutions (Hong Kong).
329 Adapter and low-quality sequences were trimmed using Trimming Galore v0.3.3. Mapping was
330 performed on TAIR10 genome annotation using Bismark v0.14.2 (Krueger & Andrews, 2011)
331 and the parameters: --bowtie2, -N 1, -p 3 (alignment); --ignore 5 --ignore_r2 5 --
332 ignore_3prime_r2 1 (methylation extractor). Only uniquely mapping reads were retained. The
333 methylKit package v0.9.4 (Akalin *et al*, 2012) was used to calculate differential methylation in
334 100 bp or 20bp non-overlapping windows (DMRs). Significance of calculated differences was
335 determined using Fisher's exact test and Benjamin-Hochberg (BH) adjustment of p-values
336 (FDR<0.05) and methylation difference cutoffs of 40% for CG, 20% for CHG and 20% for
337 CHH. Differentially methylated windows within 100bp or 20bp of each other were merged to

338 form larger DMRs. 100bp windows with at least six cytosines covered by a minimum of 6 (CG
339 and CHG) and 10 (CHH) reads in all libraries were considered.
340
341 **RNA extraction and 3'quant-seq (RNA) analyses**
342 Total RNA was extracted using Trizol followed by clean-up on RNeasy Plant Mini kit columns
343 (Macherey-Nagel). 3'end librairies were prepared using the QuantSeq 3' Fwd library prep kit
344 (Lexogen). Libraries were sequenced to acquire 150 bp-reads on a NextSeq Mid output flow
345 cell (Fasteris, Geneva). Expression level was calculated by mapping reads using STAR v2.5.3a
346 (Dobin *et al*, 2013) on the *A. thaliana* reference genome (TAIR10) with the following
347 arguments --outFilterMultimapNmax 50 --outFilterMatchNmin 30 --alignSJoverhangMin 3 --
348 alignIntronMax 10000. Counts were normalized and annotations (genes and TEs) were declared
349 differentially expressed between samples using DESeq2 (Love *et al*, 2014).
350
351 **Chromatin immunoprecipitation and ChIP-seq analyses**
352 ChIP experiments were conducted in two to four biological replicates of WT, *ddm1*, *clf* and
353 *ddm1 clf* using an anti-H3K27me3 antibody (Millipore, 07-449). For each biological replicate,
354 two IPs were carried out using 80 µg of Arabidopsis chromatin mixed with 5 µg of Drosophila
355 chromatin, as quantified using BiCinchoninic Acid assay (Thermo Fisher Scientific). DNA
356 eluted and purified from the two technical replicates was pooled before library preparation
357 (Illumina TruSeq ChIP) and sequencing (Illumina sequencing single-reads, 1 × 50 bp) of the
358 resulting input and IP samples performed by Fasteris (Geneva, Switzerland).
359 Reads were mapped using Bowtie2 v2.3.2 (Langmead & Salzberg, 2012) onto TAIR10
360 *Arabidopsis thaliana* and Drosophila melanogaster (dm6) genomes. Normalization factor (Rx)
361 for each sample using spiked-in *D. melanogaster* chromatin was calculated (Nassrallah *et al*,
362 2018) using the following formula Rx = r/Nd_IP, where Nd_IP corresponds to the number of
363 reads mapped on *D. melanogaster* genome in the IP and r corresponds to the percentage of
364 *Drosophila*-derived reads in the input. Genomic regions significantly marked by H3K27me3
365 were identify using MACS2 (Zhang *et al*, 2008) and genes or TEs overlapping these regions
366 were obtained using bedtools (Quinlan & Hall, 2010). The number of reads over marked genes
367 or TEs were normalized by applying the normalization factor and differentially marked genes
368 between samples were calculated using DESeq2 (Love *et al*, 2014).
369
370
371

372 **TE-sequence capture**

373 TE sequence capture was performed on around 100 seedlings in all cases except *ddm1-clf*#23
374 NOchl were only 12 seedlings were recovered. Seedlings were grown in plates under control
375 (long-day) conditions and genomic DNA was extracted using the CTAB method (Murray &
376 Thompson, 1980). Libraries were prepared as previously described (Quadrana *et al*, 2019) using
377 1µg of DNA and TruSeq paired-end kit (Illumina) following manufacturer instructions.
378 Libraries were then amplified through 7 cycles of ligation-mediated PCR using the KAPA HiFi
379 Hot Start Ready Mix and primers AATGATACGGCGACCACCGAGA and
380 CAAGCAGAAGACGGCATACGAG at a final concentration of 2µM. 1µg of multiplexed
381 libraries were then subjected to TE-sequence capture exactly as previously reported (Quadrana
382 *et al*, 2016). Pair-end sequencing was performed using one lane of Illumina NextSeq500 and
383 75bp reads. About 42 million pairs were sequenced per library and mapped to the TAIR10
384 reference genome using Bowtie2 v2.3.2 (Langmead & Salzberg, 2012) with the arguments --
385 mp 13 --rdg 8,5 --rfg 8,5 --very-sensitive. An improved version of SPLITREADER (available
386 at https://github.com/LeanQ/SPLITREADER) was used to detect new TE insertions. Briefly,
387 split-reads as well as discordant reads mapping partially on reference and consensus TE
388 sequences (obtained from RepBase update) were identified, soft clipped and remapped to the
389 TAIR10 reference genome using Bowtie2 (Langmead & Salzberg, 2012). Putative insertions
390 supported by at least one split- and/or discordant-reads at each side of the insertion sites were
391 retained. Insertions spanning centromeric repeats or coordinates spanning the corresponding
392 donor TE sequence were excluded. In addition, putative TE insertions detected in more than
393 one library were excluded to retain only sample-specific TE insertions.
394
395
396 **Southern blot**

397 DNA from 5 week-old rosette leaves was extracted using a standard CTAB protocol. 1,5 µg
398 of genomic DNA was digested overnight with SSpI restriction enzyme. The digestion was run
399 on a 1% agarose gel, transferred to Hybond N+ membranes, blocked and washed according to
400 manufacturer instructions (GE Healthcare). Membranes were probed with a PCR product
401 (corresponding to a fragment of *EVD* GAG sequence,) radiolabeled with alpha 32P-dCTP
402 using the Megaprime DNA Labeling System. EVD PCR product was generated with the same
403 primers as in (Marí-Ordóñez *et al*, 2013).
404
405

406 **Pyrosequencing**

407 *ATCOPIA93* DNA from gDNA (same extraction as used in Southern Blot) was analyzed as in
408 (Zervudacki *et al*, 2018).

409

410 **Cytology**

411 DAPI staining on fixed nuclei was performed as described in Bourbousse et al., 2015 using 10-
412 days-old chopped cotyledons to avoid developmental defects due to accumulation of
413 transposition. For immuno-detection, a primary antibody against H3K9me2 (Abcam 1220) at a
414 1:200dilution was used, followed by a secondary antibody (Alexa Fluor 488 mouse) at a 1:400
415 dilution and DAPI staining. Images were acquired with a confocal laser scanning microscope
416 and processed using ImageJ (https://imagej.nih.gov/ij/).

417

418 **Data availability**

419 Sequencing data has been deposited in the European Nucleotide Archive (ENA) under project
420 PRJEB34363.

421

422 **Acknowledgments**

423 We thank the Genomics and Informatics facilities at IBENS as well as the Barneche lab (C.
424 Bourbousse and G. Teano) for their help with Drosophila spike-in ChIP experiments and
425 discussions. This work was funded by a Human Frontier Scientific Program Career
426 Development Award (HFSP-CDA-00018/2014) granted to A.D and the Centre National de la
427 Recherche Scientifique (CNRS) Momentum program granted to L.Q. Additional support was
428 from the CNRS.

429

430

431

432 **Conflict of interest:** The authors declare that they have no conflict of interest.

433

434

435

436

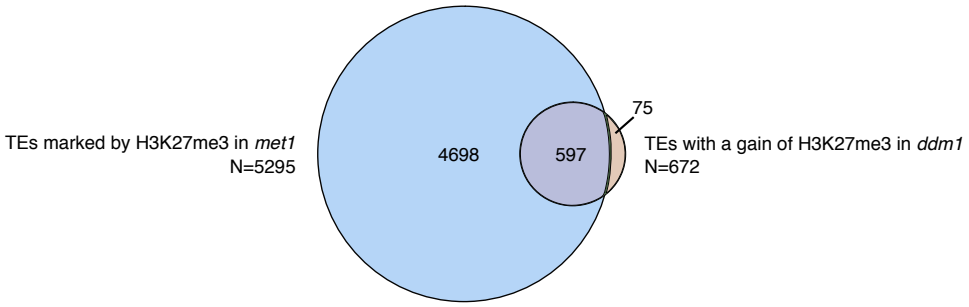

Sup Fig.1A Overlap between TEs marked by H3K27me3 in *met1* (Deleris et al., 2012) and TEs with a gain of H3K27me3 in *ddm1.*

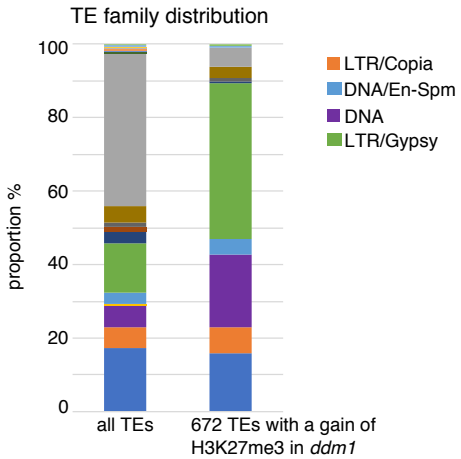

Sup Fig.1B Distribution of the different TE families among the TEs that significantly gain H3K27me3 in *ddm1* compared to the family distribution of all TEs.

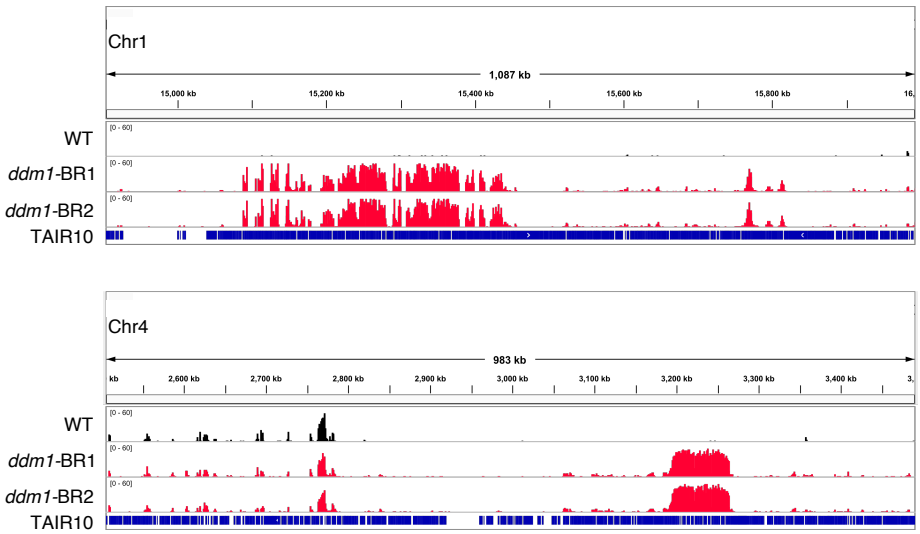

Sup Fig.1C Genome browser view of chromosomes 1 and 4 showing the two largest H3K27me3 domains in *ddm1* (BR=biological replicate).

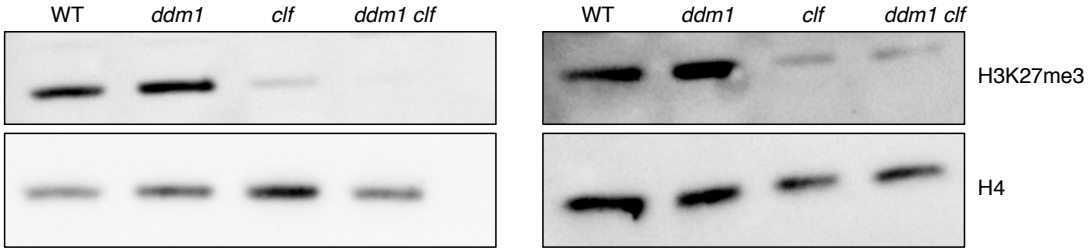

Sup Fig.2A Immuno detection of H3K27me3 in chromatin extracts (H4 is used as a loading control), two biological replicates are shown.

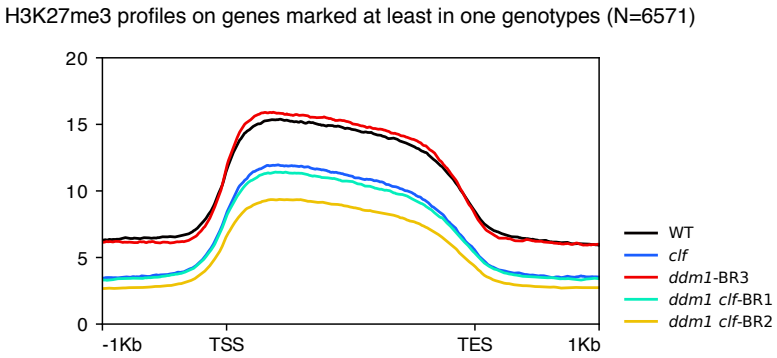

Sup Fig.2B Metagene showing H3K27me3 levels on genes marked in at least one genotype

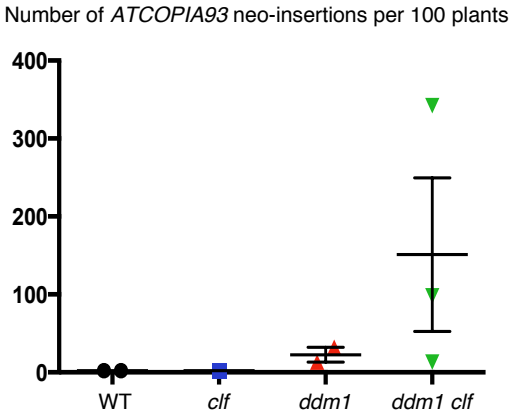

Sup Fig.3A Number of *EVD* neo-insertions revealed by TE-capture in several lines per genotype, all derived from a cross between *ddm1* and *clf* mutants.

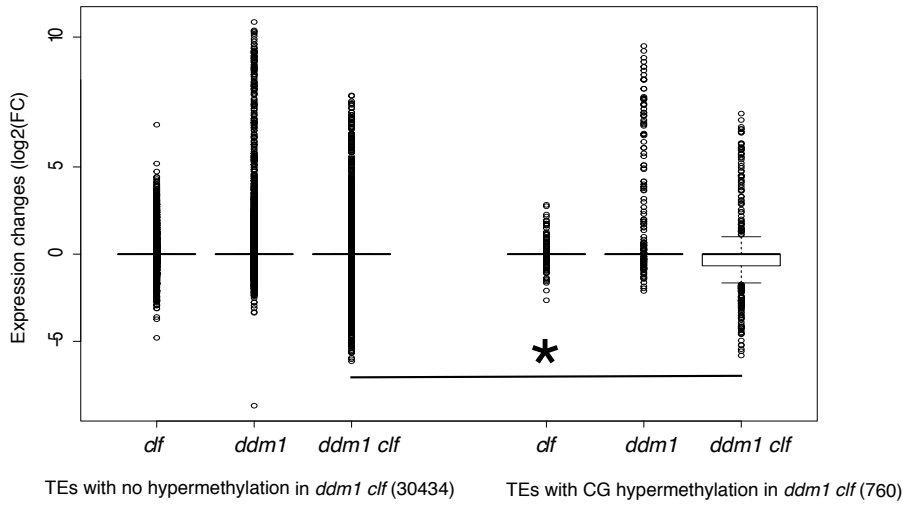

Sup Fig.5A Graph showing expression changes of TE hypermethylated or not in *ddm1 clf* in different genetic backgrounds.

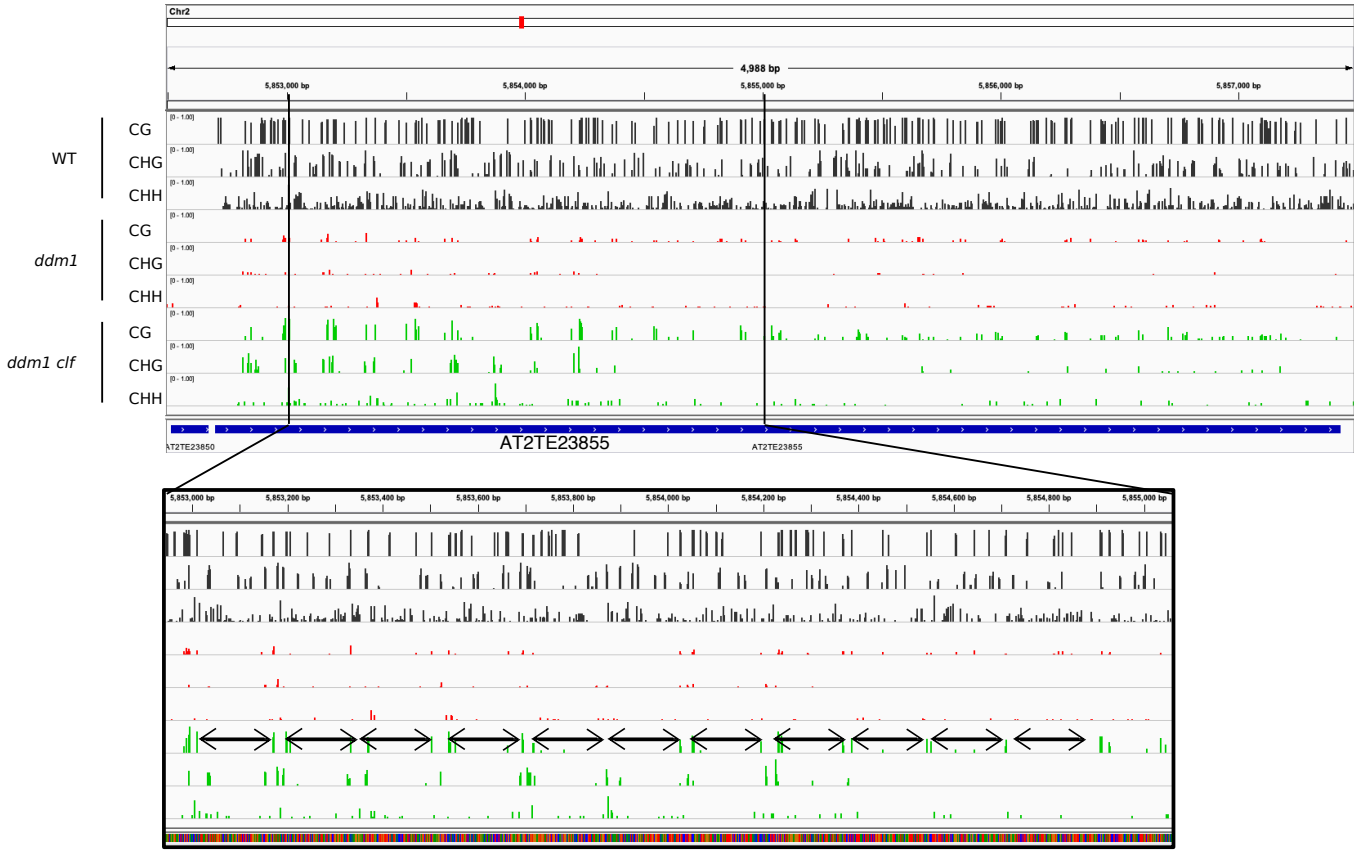

Sup Fig.5B Representative view of a TE with a periodic DNA hypermethylation every 140bp; the bottom panel is a zoom of the top pane and the double arrow represents a distance of 140bp.

437 **References**

438

439 Akalin A, Kormaksson M, Li S, Garrett-Bakelman FE, Figueroa ME, Melnick A & Mason
440 CE (2012) MethylKit: a comprehensive R package for the analysis of genome-wide
441 DNA methylation profiles. *Genome Biol.* **13:** R87 Available at:
442 http://genomebiology.com/2012/13/10/R87
443 Baillie JK, Barnett MW, Upton KR, Gerhardt DJ, Richmond TA, Sapio F De, Brennan P,
444 Rizzu P, Smith S, Fell M, Talbot RT, Gustincich S, Freeman TC, Mattick JS, Hume DA,
445 Heutink P, Carninci P, Jeddeloh JA & Faulkner GJ (2011) Somatic retrotransposition
446 alters the genetic landscape of the human brain. *Nature* **479:** 534–537 Available at:
447 http://dx.doi.org/10.1038/nature10531
448 Baroux C, Pecinka A, Fuchs J, Schubert I & Grossniklaus U (2007) The Triploid Endosperm
449 Genome of Arabidopsis Adopts a Peculiar, Parental-Dosage-
450 Dependent Chromatin Organization. *Plant Cell* **19:** 1782 LP – 1794 Available at:
451 http://www.plantcell.org/content/19/6/1782.abstract
452 Basenko EY, Sasaki T, Ji L, Prybol CJ, Burckhardt RM, Schmitz RJ & Lewis ZA (2015)
453 Genome-wide redistribution of H3K27me3 is linked to genotoxic stress and defective
454 growth. *Proc. Natl. Acad. Sci.* **112:** E6339–E6348
455 Becker, Claude Koenig D, Stegle O, Borgwardt K & Weigel D (2011) thaliana methylome.
456 Bourbousse C, Ahmed I, Roudier F, Zabulon G, Blondet E, Balzergue S, Colot V, Bowler C
457 & Barneche F (2012) Histone H2B Monoubiquitination Facilitates the Rapid Modulation
458 of Gene Expression during Arabidopsis Photomorphogenesis. *PLOS Genet.* **8:** e1002825
459 Available at: https://doi.org/10.1371/journal.pgen.1002825
460 Bouveret R, Schönrock N, Gruissem W & Hennig L (2006) Regulation of flowering time by
461 Arabidopsis MSI1. *Development* **133:** 1693–1702
462 Calarco JP, Borges F, Donoghue MTA, Van Ex F, Jullien PE, Lopes T, Gardner R, Berger F,
463 Feijó JA, Becker JD & Martienssen RA (2012) Reprogramming of DNA methylation in
464 pollen guides epigenetic inheritance via small RNA. *Cell* **151:** 194–205
465 Cao X & Jacobsen SE (2002) Role of the Arabidopsis DRM methyltransferases in de novo
466 DNA methylation and gene silencing. *Curr. Biol.* **12:** 1138–1144
467 Carter B, Bishop B, Ho K, Huang R, Jia W, Zhang H & Pascuzzi PE (2018) The Chromatin
468 Remodelers PKL and PIE1 Act in an Epigenetic Pathway That Determines H3K27me3
469 Homeostasis in Arabidopsis. **30:** 1337–1352
470 Chan SW-L (2004) RNA Silencing Genes Control de Novo DNA Methylation. *Science.* **303:**

471 1336–1336 Available at: http://www.sciencemag.org/cgi/doi/10.1126/science.1095989
472 Chanvivattana Y, Bishopp A, Schubert D, Stock C, Moon Y, Sung ZR & Goodrich J (2004)
473 Interaction of Polycomb-group proteins controlling flowering in Arabidopsis. **:** 5263–
474 5276
475 Chica C, Louis A, Roest Crollius H, Colot V & Roudier F (2017) Comparative epigenomics
476 in the Brassicaceae reveals two evolutionarily conserved modes of PRC2-mediated gene
477 regulation. *Genome Biol.* **18:** 1–15
478 Deleris A, Stroud H, Bernatavichute Y, Johnson E, Klein G, Schubert D & Jacobsen SE
479 (2012) Loss of the DNA Methyltransferase MET1 Induces H3K9 Hypermethylation at
480 PcG Target Genes and Redistribution of H3K27 Trimethylation to Transposons in
481 Arabidopsis thaliana. *PLoS Genet.* **8:** e1003062 Available at:
482 http://dx.plos.org/10.1371/journal.pgen.1003062
483 Dobin A, Davis CA, Schlesinger F, Drenkow J, Zaleski C, Jha S, Batut P, Chaisson M &
484 Gingeras TR (2013) STAR: Ultrafast universal RNA-seq aligner. *Bioinformatics* **29:** 15–
485 21
486 Du J, Johnson LM, Jacobsen SE & Patel DJ (2015) DNA methylation pathways and their
487 crosstalk with histone methylation. *Nat. Rev. Mol. Cell Biol.* **16:** 519–532 Available at:
488 http://www.nature.com/doifinder/10.1038/nrm4043
489 Förderer A, Zhou Y & Turck F (2016) The age of multiplexity: Recruitment and interactions
490 of Polycomb complexes in plants. *Curr. Opin. Plant Biol.* **29:** 169–178
491 Holoch D & Margueron R (2017) Mechanisms Regulating PRC2 Recruitment and Enzymatic
492 Activity. *Trends Biochem. Sci.* **42:** 531–542 Available at:
493 http://dx.doi.org/10.1016/j.tibs.2017.04.003
494 Ibarra CA, Feng X, Schoft VK, Hsieh TF, Uzawa R, Rodrigues JA, Zemach A, Chumak N,
495 Machlicova A, Nishimura T, Rojas D, Fischer RL, Tamaru H & Zilberman D (2012)
496 Active DNA demethylation in plant companion cells reinforces transposon methylation
497 in gametes. *Science.* **337:** 1360–1364
498 Ingouff M, Rademacher S, Holec S, Xin N, Readshaw A & Foo SH (2010) Report Zygotic
499 Resetting of the HISTONE 3 Variant Repertoire Participates in Epigenetic
500 Reprogramming in Arabidopsis. **:** 2137–2143
501 Jacob Y, Feng S, LeBlanc CA, Bernatavichute Y V, Stroud H, Cokus S, Johnson LM,
502 Pellegrini M, Jacobsen SE & Michaels SD (2009) ATXR5 and ATXR6 are H3K27
503 monomethyltransferases required for chromatin structure and gene silencing. *Nat. Struct.*
504 *Mol. Biol.* **16:** 763–768 Available at: https://www.ncbi.nlm.nih.gov/pubmed/19503079

505 Jacob Y, Stroud H, Leblanc C, Feng S, Zhuo L, Caro E, Hassel C, Gutierrez C, Michaels SD
506 & Jacobsen SE (2010) Regulation of heterochromatic DNA replication by histone H3
507 lysine 27 methyltransferases. *Nature* **466:** 987–991
508 Johnson L, Cao X & Jacobsen S (2002) Interplay between two epigenetic marks. DNA
509 methylation and histone H3 lysine 9 methylation. *Curr. Biol.* **12:** 1360–1367
510 Kankel MW, Ramsey DE, Stokes TL, Flowers SK, Haag JR, Jeddeloh JA, Riddle NC,
511 Verbsky ML & Richards EJ (2003) Arabidopsis MET1 cytosine methyltransferase
512 mutants. *Genetics* **163:** 1109–1122
513 Krueger F & Andrews SR (2011) Bismark: A flexible aligner and methylation caller for
514 Bisulfite-Seq applications. *Bioinformatics* **27:** 1571–1572
515 Langmead B & Salzberg SL (2012) Fast gapped-read alignment with Bowtie 2. *Nat. Methods*
516 **9:** 357–9
517 Li Y, Zheng H, Wang Q, Zhou C, Wei L, Liu X, Zhang W, Zhang Y, Du Z, Wang X & Xie
518 W (2018) Genome-wide analyses reveal a role of Polycomb in promoting
519 hypomethylation of DNA methylation valleys. *Genome Biol.* **19:** 1–16
520 Lippman Z, Gendrel A-V, Black M, Vaughn MW, Dedhia N, Richard McCombie W, Lavine
521 K, Mittal V, May B, Kasschau KD, Carrington JC, Doerge RW, Colot V & Martienssen
522 R (2004) Role of transposable elements in heterochromatin and epigenetic control.
523 *Nature* **430:** 471–476 Available at:
524 http://www.nature.com/doifinder/10.1038/nature02651
525 Love MI, Huber W & Anders S (2014) Moderated estimation of fold change and dispersion
526 for RNA-seq data with DESeq2. *Genome Biol.* **15:** 550
527 Lyons DB & Zilberman D (2017) DDM1 and Lsh remodelers allow methylation of DNA
528 wrapped in nucleosomes. **:** 1–20
529 Makarevich G, Villar CBR, Erilova A & Köhler C (2008) Mechanism of PHERES1
530 imprinting in Arabidopsis. **1:** 906–912
531 Marasca F, Bodega B & Orlando V (2018) How Polycomb-Mediated Cell Memory Deals
532 With a Changing Environment. *BioEssays* **40:** 1700137 Available at:
533 https://doi.org/10.1002/bies.201700137
534 Marí-Ordóñez A, Marchais A, Etcheverry M, Martin A, Colot V & Voinnet O (2013)
535 Reconstructing de novo silencing of an active plant retrotransposon. *Nat. Genet.* **45:**
536 1029–1039 Available at: http://www.nature.com/doifinder/10.1038/ng.2703
537 Martínez G, Panda K, Köhler C & Slotkin RK (2016) movement from the surrounding nurse
538 cell. *Nat. Plants* **2:** 1–8 Available at: http://dx.doi.org/10.1038/nplants.2016.30

539 Mathieu O, Probst A V & Paszkowski J (2005) Distinct regulation of histone H3 methylation
540 at lysines 27 and 9 by CpG methylation in Arabidopsis. *EMBO J.* **24:** 2783–2791
541 Available at: http://emboj.embopress.org/cgi/doi/10.1038/sj.emboj.7600743
542 Murray G & Thompson WF (1980) Rapid isolation of high molecular weight plant DNA.
543 *Nucleic Acids Res.* **8:** 4321–4326
544 Nassrallah A, Rougée M, Bourbousse C, Drevensek S, Fonseca S, Iniesto E, Ait-Mohamed O,
545 Deton-Cabanillas AF, Zabulon G, Ahmed I, Stroebel D, Masson V, Lombard B,
546 Eeckhout D, Gevaert K, Loew D, Genovesio A, Breyton C, de Jaeger G, Bowler C, et al
547 (2018) DET1-mediated degradation of a SAGA-like deubiquitination module controls
548 H2Bub homeostasis. *Elife* **7:** 1–29
549 Orlando DA, Chen MW, Bradner JE, Guenther MG, Orlando DA, Chen MW, Brown VE,
550 Solanki S, Choi YJ & Olson ER (2014) Quantitative ChIP-Seq Normalization Reveals
551 Global Modulation of the Epigenome Resource Quantitative ChIP-Seq Normalization
552 Reveals Global Modulation of the Epigenome. *CellReports* **9:** 1163–1170 Available at:
553 http://dx.doi.org/10.1016/j.celrep.2014.10.018
554 Prete S, Mikulski P, Schubert D & Gaudin V (2015) One, Two, Three: Polycomb Proteins Hit
555 All Dimensions of Gene Regulation. **:** 520–542
556 Quadrana L, Bortolini Silveira A, Mayhew GF, LeBlanc C, Martienssen RA, Jeddeloh JA &
557 Colot V (2016) The Arabidopsis thaliana mobilome and its impact at the species level.
558 *Elife* **5:** 1–25 Available at: http://elifesciences.org/lookup/doi/10.7554/eLife.15716
559 Quadrana L, Etcheverry M, Gilly A, Caillieux E, Madoui M-A, Guy J, Bortolini Silveira A,
560 Engelen S, Baillet V, Wincker P, Aury J-M & Colot V (2019) Transposition favors the
561 generation of large effect mutations that may facilitate rapid adaption. *Nat. Commun.* **10:**
562 1–10 Available at: http://dx.doi.org/10.1038/s41467-019-11385-5
563 Quinlan AR & Hall IM (2010) BEDTools: A flexible suite of utilities for comparing genomic
564 features. *Bioinformatics* **26:** 841–842
565 Reddington JP, Perricone SM, Nestor CE, Reichmann J, Youngson NA, Suzuki M, Reinhardt
566 D, Dunican DS, Prendergast JG, Mjoseng H, Ramsahoye BH, Whitelaw E, Greally JM,
567 Adams IR, Bickmore WA & Meehan RR (2013) Redistribution of H3K27me3 upon
568 DNA hypomethylation results in de-repression of Polycomb target genes. *Genome Biol.*
569 **14:** R25 Available at: http://genomebiology.biomedcentral.com/articles/10.1186/gb-
570 2013-14-3-r25
571 Rodrigues JA & Zilberman D (2015) Evolution and function of genomic imprinting in plants.
572 **:** 2517–2531

573 Saksouk N, Barth TK, Ziegler-Birling C, Olova N, Nowak A, Rey E, Mateos-Langerak J,
574 Urbach S, Reik W, Torres-Padilla ME, Imhof A & Déjardin J (2014) Redundant
575 Mechanisms to Form Silent Chromatin at Pericentromeric Regions Rely on BEND3 and
576 DNA Methylation. *Mol. Cell* **56:** 580–594
577 She W, Grimanelli D & Baroux C (2014) An efficient method for quantitative , single-cell
578 analysis of chromatin modification and nuclear architecture in whole-mount ovules in
579 arabidopsis An Efficient Method for Quantitative , Single-cell Analysis of Chromatin
580 Modification and Nuclear Architect. **:** 1–9
581 Shengbo He, Martin Vickers, Jingyi Zhang XF (2019) Natural depletion of H1 in sex cells
582 causes DNA demethylation, heterochromatin decondensation and transposon activation.
583 *bioRxiv***:** 1–11 Available at:
584 https://www.biorxiv.org/content/biorxiv/early/2018/10/26/451930.full.pdf
585 Slotkin RK, Vaughn M, Borges F, Tanurdžić M, Becker JD, Feijó JA & Martienssen RA
586 (2009) Epigenetic Reprogramming and Small RNA Silencing of Transposable Elements
587 in Pollen. *Cell* **136:** 461–472
588 Soppe WJJ, Jasencakova Z, Houben A, Kakutani T, Meister A, Huang MS, Jacobsen SE,
589 Schubert I & Fransz PF (2002) DNA methylation controls histone H3 lysine 9
590 methylation and heterochromatin assembly in Arabidopsis. **21:** 6549–6559
591 Stroud H, Do T, Du J, Zhong X, Feng S, Johnson L, Patel DJ & Jacobsen SE (2014) Non-CG
592 methylation patterns shape the epigenetic landscape in Arabidopsis. *Nat. Struct. Mol.*
593 *Biol.* **21:** 64–72 Available at: http://www.ncbi.nlm.nih.gov/pubmed/24336224
594 Tsukahara S, Kobayashi A, Kawabe A, Mathieu O, Miura A & Kakutani T (2009) Bursts of
595 retrotransposition reproduced in Arabidopsis. *Nature* **461:** 423–426 Available at:
596 http://www.nature.com/doifinder/10.1038/nature08351
597 Vongs A, Kakutani T, Martienssen RA & Richardstt EJ (1993) Arabidopsis thaliana DNA
598 Methylation Mutants. *Science.* **260:** 1926–1928
599 Walter M, Teissandier A, Pérez-Palacios R & Bourc'His D (2016) An epigenetic switch
600 ensures transposon repression upon dynamic loss of DNA methylation in embryonic
601 stem cells. *Elife* **5:** 1–30
602 Wang H, Liu C, Cheng J, Liu J, Zhang L, He C, Shen WH, Jin H, Xu L & Zhang Y (2016)
603 Arabidopsis Flower and Embryo Developmental Genes are Repressed in Seedlings by
604 Different Combinations of Polycomb Group Proteins in Association with Distinct Sets of
605 Cis-regulatory Elements. *PLoS Genet.* **12:** 1–25
606 Weinhofer I, Hehenberger E, Roszak P, Hennig L & K??hler C (2010) H3K27me3 profiling

607 of the endosperm implies exclusion of polycomb group protein targeting by DNA
608 methylation. *PLoS Genet.* **6:** 1–14
609 Xiao J, Jin R, Yu X, Shen M, Wagner JD, Pai A, Song C, Zhuang M, Klasfeld S, He C,
610 Santos AM, Helliwell C, Pruneda-Paz JL, Kay SA, Lin X, Cui S, Garcia MF, Clarenz O,
611 Goodrich J, Zhang X, et al (2017) Cis and trans determinants of epigenetic silencing by
612 Polycomb repressive complex 2 in Arabidopsis. *Nat. Genet.* **49:** 1546–1552 Available at:
613 http://www.nature.com/doifinder/10.1038/ng.3937
614 Yang H, Yang H, Berry S, Olsson TSG, Hartley M, Howard M & Dean C (2017) Distinct
615 phases of Polycomb silencing to hold epigenetic memory of cold in Arabidopsis.
616 *Science.* **1121:** 1–9
617 Zemach A, Kim MY, Hsieh PH, Coleman-Derr D, Eshed-Williams L, Thao K, Harmer SL &
618 Zilberman D (2013) The arabidopsis nucleosome remodeler DDM1 allows DNA
619 methyltransferases to access H1-containing heterochromatin. *Cell* **153:** 193–205
620 Available at: http://dx.doi.org/10.1016/j.cell.2013.02.033
621 Zervudacki J, Yu A, Amesefe D, Wang J, Drouaud J, Navarro L & Deleris A (2018)
622 Transcriptional control and exploitation of an immune-responsive family of plant
623 retrotransposons. *EMBO J.* **37:** e98482 Available at:
624 http://emboj.embopress.org/lookup/doi/10.15252/embj.201798482
625 Zhang Y, Liu T, Meyer CA, Eeckhoute J, Johnson DS, Bernstein BE, Nussbaum C, Myers
626 RM, Brown M, Li W & Shirley XS (2008) Model-based analysis of ChIP-Seq (MACS).
627 *Genome Biol.* **9:**
628 Zilberman D, Coleman-Derr D, Ballinger T & Henikoff S (2008) Histone H2A.Z and DNA
629 methylation are mutually antagonistic chromatin marks. *Nature* **456:** 125–129 Available
630 at: https://www.ncbi.nlm.nih.gov/pubmed/18815594
631